Energy, Mines and Resources Canada | Énergie, Mines et Ressources Canada

CANMET

Canada Centre for Mineral and Energy Technology | Centre canadien de la technologie des minéraux et de l'énergie

CHARACTERIZATION OF LONG-LIVED RADIOACTIVE DUST CLOUDS GENERATED IN MECHANICAL OPERATIONS IN A URANIUM MILL

J. BIGU AND E. EDWARDSON

ELLIOT LAKE LABORATORY

OCTOBER 1986

MINING RESEARCH LABORATORIES
DIVISION REPORT MRL 87-65 (TR)

MRL 87-65(TR) c. 2

CHARACTERIZATION OF LONG-LIVED RADIOACTIVE DUST CLOUDS GENERATED IN MECHANICAL OPERATIONS IN A URANIUM MILL

by

J. Bigu* and E. Edwardson**

ABSTRACT

The characteristics of long-lived radioactive dust clouds generated in several mechanical operations in a uranium mill have been investigated. The study consisted of the determination of dust size distribution, and of the size distribution of radionuclides associated with particulate matter in the size range 0.1 to 26 μm. Experiments were conducted using several cascade impactors operating at different sampling rates, and with different numbers of impactor stages. Two different types of cascade impactors were used. Radionuclide identification was done using α-spectrometry and γ-spectrometry. Long-lived and short-lived radionuclides were identified in dust samples. The characteristics of the dust clouds depended on the mechanical operation. The following mechanical operations were studied: crushing (vibrating grizzly, jaw crusher, cone crusher); screening; ore transportation; grinding; and yellowcake packaging. In addition, other dust and radioactivity measurements have been carried out.

Keywords: Radioactivity; Dust; Uranium; Mill.

*Research Scientist and Radiation/Respirable Dust/Ventilation Project Leader, ** Technologist, Elliot Lake Laboratory, CANMET, Energy, Mines and Resources Canada, Elliot Lake, Ontario.

CARACTÉRISATION DES ÉMISSIONS DE POUSSIÈRES RADIOACTIVES À LONGUE PÉRIODE AU COURS DES OPÉRATIONS MÉCANIQUES D'UN BROYEUR D'URANIUM

par

J. Bigu* et E. Edwardson**

RÉSUMÉ

Les auteurs ont étudié les caractéristiques des nuages de poussière radioactive à longue période produits au cours des nombreuses opérations mécaniques d'un broyeur d'uranium. L'étude avait pour objet de déterminer la distribution granulométrique de la poussière ainsi que la distribution granulométrique des radionucléides associées à la matière subdivisée dans la plage des particules de <0,1 à 26 µm. On a fait des essais avec deux genres différents d'impacteurs à cascade fonctionnant à différentes vitesses d'écoulement échantillonnées. L'identification des radionucléides a été réalisée par spectrométrie α et par spectrométrie γ. Des radionucléides à longue période et à courte période ont été identifiées dans les échantillons de poussière. Les caractéristiques des nuages de poussières dépendent de l'opération mécanique. On a donc étudié les opérations mécaniques suivantes: le concassage (crible à barres, concasseur à mâchoires, concasseur à cônes); le criblage; le transport du minerai; le broyage, et l'emballage du concentré d'uranium. Enfin, d'autres mesures de poussières et de rayonnement ont été effectuées.

Mots-clés: Rayonnement; Poussière; Uranium; Broyeur

*Chercheur scientifique, et Chef de projet Rayonnement/Poussières respirables/Ventilation;

**Technologiste, CANMET, Énergie, Mines et Ressources Canada, Elliot Lake, Ontario.

INTRODUCTION

Inhalation of airborne radioactive contaminants poses a health risk to occupational workers. Because of this, monitoring of radioactivity concentrations and dust levels for dose exposure calculation purposes is a subject of great practical interest.

Until recently, the short-lived decay products of radon were the only airborne radioisotopes of concern from the occupational health viewpoint in uranium mines and mills. However, increasing experimental evidence indicates that attention should also be paid to the short-lived decay products of thoron, in some uranium mines, and the long-lived radioisotopes (U-235, U-238 and Th-232 and some of their decay products) associated, respectively, with aerosols in the submicron range and dust in the respirable size range. Some recent concern has been expressed particularly with regard to the inhalation of respirable dust (1-10 μm) containing long-lived radioisotopes, as once inhaled and lodged in tissue they will remain active for long periods until eliminated by natural biological processes.

Although measurements have been conducted to determine the aerosol size distribution associated with the short-lived decay products of radon and thoron (1-4), more studies are necessary. Furthermore, very little information is available regarding the long-term effects of continuous exposure to long-lived radioactive dust (LLRD). Sparse data are also available on LLRD size distribution in uranium mines and mills. Thus, it is important to identify the main radioisotopes in LLRD, their concentration in air and their size distribution as the latter determines the attachment characteristics of LLRD in the respiratory system (5-7).

This report presents experimental data collected in a uranium mill. Long-lived radioactive dust is generated in the course of mechanical and

physico-chemical unit operations carried out in the separation and refining processes of uranium, or uranium chemical compounds, from uranium ores. The data presented in this report correspond to the mechanical operations of the mill which include transportation by conveyor belts, crushing, grinding, screening (i.e., sizing), and packaging operations. Measurements were conducted on:

a) Long-lived radioactivity associated with dust in the 1-30 μm size range and short-lived radon progeny radioactivity associated with airborne particulates in the same size range, and in the submicron range.

b) Concentration and size distribution of airborne particulate matter in the submicron and 1-30 μm range.

EXPERIMENTAL APPARATUS AND METHODS

Size distribution analyses of radioactive dust, radioactive aerosol and dust were conducted by means of two 10-stage, radial slot-design, cascade impactors, model 210, manufactured by Sierra Instruments Inc. (U.S.A), now Anderson. One cascade impactor was operated with 10-stages, whereas the other cascade impactor was operated with only 8-stages. In the latter case, the last two ultrafine impactor stages were eliminated at the expense of losing some size distribution information, but with the obvious benefit of substantially increasing the amount of dust collected on the remaining 8 impactor stages. In a few cases both impactors were operated with 8-stages. Glass fiber filters (47 mm diameter), with radial slot-design similar to that of the cascade impactor stages, were used as substrates to collect the samples. The cascade impactors were operated for about 12 hours at a time. The impactors were operated at the following sampling rates: 10.4 L/min (8-stage), and 3.3 L/min (10-stage).

The glass fiber substrates placed behind the stages of the cascade

impactors enabled determination of the size distribution (mass median aerodynamic diameter, MMAD, and geometric standard deviation) of dust by determining the weight of the filters before and after the sampling period. The substrates were dried before and after sampling to eliminate moisture. Ambient temperature and pressure were carefully noted during sampling and results were corrected according to standard operating procedures. Total dust was also estimated from cascade impactor data.

Radioactivity (α-particle) measurements on the impactor substrates also enabled calculation of the long-lived radioactive dust (LLRD), and radon progeny, size distribution, i.e., activity median aerodynamic diameter, AMAD, and geometric standard deviation.

Also used in the determination of LLRD and radon progeny size distribution was one small 8-stage, personal Marple cascade impactor. This impactor differs significantly from the Sierra impactors in a number of ways such as size, weight and geometry. The Marple impactors are much smaller and lighter than the Sierra impactors. The impactor stages slot design is also different, i.e., six radial slots for the Marple impactors, as opposed to four radial slots for the Sierra impactors. The Marple impactors were operated at a nominal flow-rate of 2 L/min. Stainless steel substrates were used as dust collectors. Because of the low flow-rate at which these impactors are operated, and the relatively large weight of the substrates, as compared with glass fiber filters, no attempt was made to measure dust, only the radioactivity associated with it.

The total LLRD and radon progeny concentrations were also estimated from impactor data. The radon progeny was measured about 40 min after sampling. A counting time of 5 min was chosen. The α-particle activity of the LLRD was measured 1-2 weeks after sampling to allow the radon progeny and thoron progeny, if any, to decay away completely. Because of the low LLRD

activity, each sample was counted several times for 30 min each time, and the average value, after subtracting the background, was used in the calculations.

The procedure used for the determination of dust, activity and size distribution from the cascade impactor data was as follows:

1. Activity (dpm, i.e., disintegrations per min) and dust mass collected on each impactor stage were carefuly noted.
2. Total activity and total dust mass from all the stages of the impactor, including the backfilter (BF), were estimated.
3. Percentage (%) activity and % dust mass for each impactor stage were calculated.
4. Cumulative % of dust mass and cumulative % of activity, less than $D_{p,50}$ (see below), were estimated as follows. Dust mass (or activity) % of the BF was used as cumulative % for the last ultrafine stage, i.e., stage 8, or stage 10. The cumulative % for the next stage was obtained by adding the % of dust mass (or activity) to the cumulative % dust mass (or activity) corresponding to the previous stage, and so on.
5. Cumulative % dust mass (or activity), less than $D_{p,50}$, versus EAD was plotted.

The variable $D_{p,50}$ is defined as the particle size cut-off at 50% collection efficiency for spherical particles. The magnitude EAD is the Equivalent Aerodynamic Diameter defined as the size of a spherical particle of density 1 g/cm^3 which has the same terminal settling velocity as the sampled particle.

In addition to gross α-counting, alpha- and gamma-spectrometry was also conducted on several dust samples using, respectively, a silicon-barrier detector (SiBD) and a high-purity Germanium detector (HPGD).

Radon daughter Working Levels, WL, were monitored as several locations in the mill using a continuous WL-monitor, and by grab-sampling using the

Thomas-Tsivoglou method. Respirable dust was measured using nylon cyclone samplers. Total dust was determined by open-face filter techniques.

Dust generated by mechanical operations in a uranium mill was sampled at several transfer points and locations in the mill. A brief description of the mechanical operations of the mill are given below.

MECHANICAL OPERATIONS

Uranium ore from an ore pit and a nearby uranium mine was dumped by a truck loader into a piston-type rock breaker, i.e., 'vibrating grizzly', where the ore was broken into smaller sizes and dropped into a chute which fed a conveyor belt. Ore smaller than a given size was shaken directly into the chute. Sampling was done at the grizzly/conveyor belt transfer point which will be denoted hereafter as transfer point 1 (TP1).

Crushed ore from the grizzly was transferred to a jaw-crusher via a vibrating screen where finer ore drops through by-passing the second crushing operation. Coarser ore is further crushed to a smaller size by the jaw-crusher. Ore passing through the vibrating screen and the crusher is transported by a conveyor belt to special screens for size selection. Sampling in this area was done below the jaw-crusher feeding point, but above the transfer point onto the conveyor belt. This location will be denoted hereafter as transfer point 2 (TP2).

Ore from the jaw-crusher operation was fed onto a set of screens where the fines passed directly through to a conveyor belt and was stored in fine ore bins ready for grinding. The coarser ore was fed into a cone-crusher. Sampling was conducted in an area adjacent to the screens at the same level. This will be denoted as transfer point 3 (TP3).

Ore from the screens was further reduced in size by a cone-crusher and fed to a conveyor belt which was routed back to the screening operation.

Sampling was carried out at the base of the cone-crusher, below and away from the feed point. This sampling location will be referred to as transfer point 4 (TP4).

Ore from the cone-crusher/screen system was delivered to the top of fine ore bins, for storage, by a 150 m long conveyor belt. The ore was then fed from the base of the fine ore bins to grinding for further ore size reduction. Sampling was done at the end of the long conveyor belt on top of the fine ore bins. This sampling location will be referred to as transfer point 5 (TP5).

Uranium ore was reduced to its final size by means of grinding with steel balls and cylinders. Sampling was conducted beside the grinder, i.e., transfer point 6 (TP6).

From the grinder onward the ore underwent a number of physico-chemical operations before its final processed stage in the mill, i.e., as yellowcake, and subsequent packaging in the packaging plant. Sampling was done in the packaging plant where the yellowcake was packaged in special drums for shipping to the refinery for further processing and purification in the fuel fabrication cycle. Sampling at this location will be referred to as transfer point 7 (TP7).

Figure 1 shows a flow diagram of the mill where measurements were carried out. The flow diagram includes mechanical and physico-chemical operations.

EXPERIMENTAL RESULTS AND DISCUSSION

Measurements were conducted during March and June 1986. Three cascade impactors were used, namely: the two Sierra impactors labelled EMR and C, and one Marple impactor labelled M_2. During March, the EMR and C impactors were operated with 10-stages and 8-stages, respectively. During June, the EMR

impactor was operated with 8-stages. Furthermore, the two impactors were located side by side at each sampling station during the March measurements. The purpose of this was twofold: to determine if the number of stages would affect the MMAD and AMAD, and to obtain two samples in the same location for statistical purposes.

The data obtained have been summarized in Tables 1 and 2, and Figures 2 to 17.

Table 1 shows the operating characteristics of the three cascade impactors used. This table also shows that the cut-off sizes for the Marple impactor M_2 (2 L/min) are roughly similar to the cut-off sizes of the EMR impactor (3.3 L/min) for the same corresponding stage. The cut-off sizes of the M_2 (8-stages) are significantly higher than the cut-off sizes of C (8-stages).

Table 2 shows cascade impactor data for the long-lived radioactive dust and the radon progeny. The data included are MMAD, AMAD, geometric standard deviations, dust concentration, LLRD concentration, and the specific activity associated with dust.

Examination of Table 2 shows the following features of interest:

1. The AMAD corresponding to the LLRD is the same, or slightly larger, than the corresponding MMAD of the carrier dust.
2. The MMAD decreases as the ore is crushed, screened and ground in the different mechanical operations in the mill. The MMAD follows the natural sequence of fragmentation from the vibrating grizzly to the grinding operations. The approximate range of values for the MMAD was 3-15 μm.
3. As for the MMAD, the values for the AMAD (LLRD) depended on the type of mechanical operation. The range of values found was approximately 3.7 to 19 μm.
4. Significant differences in the values of the MMAD were found in samples

taken at the same location with impactors operated with different numbers of stages and air flows (12% to >50%). The same applies to the AMAD. There is no satisfactory explanation for the large discrepancy found between the EMR and M_2 impactors data collected during the grinding operation. However, the data corresponding to the EMR impactor are presumed to be more consistent with this milling operation.

5. As expected, the AMAD corresponding to the radon progeny associated with dust was much less than its corresponding MMAD. The AMAD obtained was in the range 0.15 to 0.7 μm, indicating that the radon progeny is preferentially associated with submicron particulate matter.
6. The quite significant differences in dust concentration, measured in high dust-production areas of the mill, by the EMR and C cascade impactors are most probably related to the stages cut-off sizes (see Table 1) and the MMAD of the dust cloud (see Table 2). It should be noted that the dust concentration ratio between the C and EMR impactors is $\lesssim$2.0, whereas the ratio for their respective sampling flow-rates is about 3.2.
7. Total dust concentration ranged widely depending on the mill (mechanical) operations. It was highest at the vibrating grizzly and for the packaging operations ($\geq$6 mg/m^3) followed by the jaw crusher ($\geq$1.5 mg/m^3). Radioactivity measurements of the specific concentration of airborne dust show, however, that gross α-activity was not linearly proportional to the amount of dust collected on the impactors substrates. It was found that the ratio of α-activity to dust mass decreased as the latter increased. These results suggest significant α-particle absorption in dust. From these data it may be concluded that although relatively high dust mass is preferable to low dust mass for MMAD calculations, this may lead to substantial α-particle self-absorption, and hence to an underestimation of airborne radioactivity concentration. It may also lead to significant

errors in the determination of the AMAD. It is presumed that the contribution to the LLRD concentration (mBq/m^3) and its specific concentration (mBq/mg), from some cascade impactor stages, may have been underestimated for mill operations that generated substantial amounts of dust.

Self-absorption problems can be minimized by choosing sampling times to ensure that adequate amounts of dust will be collected for accurate MMAD determination, while at the same time consistent with low α-particle absorption necessary for reliable measurements of the AMAD. It should be noted that during March dust concentrations were much higher than in June when doors and windows remained open day and night. This should be taken into consideration when examining Table 2 and data for the physico-chemical mill operations reported elsewhere (8).

Identification of the radionuclides in the radioactive dust was done by means of α-spectrometry and γ-spectrometry.

Alpha-spectrometry on at least one sample of each mechanical operation was carried out under vacuum conditions in order to improve the energy resolution of the spectra. Except for yellowcake samples, counting times in excess of 24 h were necessary for good counting statistics.

Because of: a) self-absorption effects, i.e., α-particle absorption in dust, leading to spectrum broadening and photopeak overlapping; b) relatively low signal-to-noise ratio; and c) spectrometer drift, positive identification of the radionuclides in dust samples by α-spectrometry was not straight forward. An ^{241}Am source, and a $^{226}Ra/^{232}Th$ source were used before and after each radioactive measurement of each dust sample. The above radioactive sources provided the following α-energy lines for α-particle identification and α-spectrometer calibration purposes:

$$^{241}Am \quad : \quad E_{\alpha} = 5.45 \text{ MeV}$$

^{218}Po : E_α = 6.0 MeV

^{214}Po : E_α = 7.69 MeV

^{212}Po : E_α = 8.78 MeV

Analysis of the data showed three main photopeaks with the following α-particle average energies: 4.13 $\pm$ 0.22 MeV, 4.75 $\pm$ 0.32 MeV, and 7.17 $\pm$ 0.3 MeV, which can tentatively be ascribed to ^{238}U (4.3 MeV), ^{226}Ra (4.8 MeV) and ^{214}Po (7.69 MeV).

The above radioisotope identification assumes no thorium present in the dust samples. This assumption is supported by open-face grab-sampling radon progeny measurements 40 min and 7 h after sampling. These measurements showed negligible residual α-activity after the radon progeny decayed away. Identification of the high energy α-particle peak was difficult because of spectral broadening and poor statistics of counting. The contribution from ^{222}Rn (5.48 MeV) and ^{218}Po (6.00 MeV) in the samples to the α-spectrum could not be ascertained because of photopeak broadening and overlapping.

Figures 2 shows two α-particle spectra corresponding to a yellowcake sample collected in the yellowcake packaging operation and a dust sample taken during the cone crushing operation, respectively. Table 3 shows the α-particle energy corresponding to the Uranium and Thorium natural series.

Dust samples from all the mill operations were analyzed by γ-spectrometry. However, despite the very high energy resolution of the apparatus (0.5 keV/channel), positive identification of the radionuclides in the dust samples was rather difficult even after counting for up to an 8 h period. The reason for this is the low radioactivity in the samples and the relatively large natural background. The activity of the sample is related to the sampling time which determines the amount of dust collected at a given flow-rate, and the ore grade.

Although many photopeaks were found in the samples, only the following

radioisotopes could be identified with reasonable certainty: ^{234}Th, ^{226}Ra, ^{214}Pb and ^{210}Pb, as belonging to the samples and not to background. Table 4 shows γ-ray energies corresponding to some radioisotopes of interest of the natural uranium radioactive chain.

Figures 3 to 8 show the cumulative dust mass percentage of size less than $D_{p,50}$ versus $D_{p,50}$, from samples taken with the two Sierra cascade impactors, EMR and C, at several transfer points, i.e., locations in the mill. As indicated above, the MMAD calculated from these data, for the two cascade impactors, differed in most cases by a substantial amount, although the two instruments were located side by side, and hence sampling took place under practically identical conditions.

Figures 9 to 15 and Figure 17 show the cumulative LLRD α-particle activity percentage associated with dust of size less than $D_{p,50}$ versus $D_{p,50}$, for the Sierra impactors. Also shown in Figures 9, 10, 12, 14, 15 and 17 is the cumulative short-lived α-particle activity percentage associated with particulate matter of size less than $D_{p,50}$ versus $D_{p,50}$, for the same impactors. The short-lived α-particle activity referred to above corresponds to the radon progeny associated with particulate matter of size less than 1 μm. As for the MMAD, case, AMAD for the LLRD and radon progeny differed quite substantially for the two cascade impactors.

Figure 16 shows the cumulative LLRD activity percentage associated with dust of size less than $D_{p,50}$ versus $D_{p,50}$, for an 8-stage Marple cascade impactor. The graphs show the uncorrected and corrected results. Data were corrected to take into account the different dust deposition efficiency in each impactor stage. The clearly curve-shaped graphs obtained for the uncorrected and corrected data are not clearly understood, but they seem to consist of two straight lines, i.e., log-normal, distributions meeting at $D_{p,50} \sim 6$ μm. The α-particle activity/dust size distribution obtained with

the Marple impactor is quite different from the distribution obtained with the Sierra impactors. Although the shape of the graphs obtained with the Marple impactor cannot satisfactorily be explained at present, it is consistent with other measurements carried out in the mill during the monitoring of some physico-chemical operations, reported elsewhere (8). It should also be noted that the AMAD obtained with the Marple impactor was much larger than that obtained with the Sierra impactor (see Table 2).

We can offer no satisfactory explanation for the different performance obtained with:

a) the same type of cascade impactor sampling at the same location but at different sampling flow-rates and with different numbers of impactor stages; and

b) different type of cascade impactors, i.e., Sierra and Marple impactors, sampling side by side.

It is not clear whether the differences observed in AMAD, MMAD and size distribution can be ascribed to differences in dust deposition patterns arising from different operating conditions, or to differences in the geometry of the cascade impactors used. This subject will be dealt with in more detail in a forthcoming report.

Table 5 shows total and respirable dust measurements at several mill operations. The values for total dust are in fair agreement with data using the cascade impactors (see Table 2). Respirable dust concentration was, of course, substantially lower than total dust concentration.

Radon progeny data at several mill locations are shown in Tables 6 and 7. Radon progeny Working Level data ranged from a few mWL up to about 67 mWL. The relatively low values for the ratios $[^{214}Pb]/[^{218}Po]$ and $[^{214}Bi]/[^{218}Po]$, in most cases, indicate the presence of reasonably 'young' air, as expected in a well ventilated area. The data for the yellowcake packaging operation have

been calculated assuming that the α-count recorded arises from ^{218}Po and ^{214}Po. This is, at least partly, not the case and the data reflect this fact. Most of the α-count arises from long-lived radioisotopes in the dust. Some negative data elsewhere reflect poor statistics of counting because of low activity levels.

SUMMARY AND CONCLUSIONS

From this study the following conclusions can be drawn. The AMAD corresponding to the long-lived radioactive dust was the same or slightly larger than the corresponding MMAD of the carrier dust.

The MMAD and AMAD calculated for the dust cloud depended on the type of mechanical operation in the mill. The values for these two diameters were in the range 3 to 19 μm.

The AMAD corresponding to the radon progeny was in the submicron range, i.e., 0.15 to 0.7 μm.

Differences were found for the MMAD and AMAD obtained at the same location with different types of cascade impactors, or using the same kind of impactors but sampling under different operating conditions. It is suggested that this topic should be further investigated.

The dust concentration depended on the mechanical operation. It was highest for the grizzly (TP1), and yellowcake packaging (TP7) operation, followed by some crushing operations, e.g., jaw-crusher (TP2).

Alpha-particle self-absorption, i.e., absorption in dust, was a problem for some samples when the mass collected in some impactor stages, in certain mechanical operations, was higher than a critical value. Hence, errors should be minimized by choosing sampling times consistent with adequate dust mass collection for accurate calculation of the MMAD, and low α-particle self-absorption for precise determination of the AMAD.

Identification of radionuclides by α-spectrometry and γ-spectrometry was not straight forward, partly because of the low specific activity of some of the samples, and other factors discussed above. The following radionuclides were identified: ^{238}U, ^{226}Ra, ^{214}Po, ^{234}Th, ^{214}Pb and ^{210}Pb.

In a forthcoming report data obtained in the same mill for the different physico-chemical mill operations will be presented and discussed.

ACKNOWLEDGEMENTS

This study was requested and partly supported by Atomic Energy Control Board (AECB). The authors are particularly grateful to Dr. H. Stocker and Dr. P. Duport for their interest and support in this work. The authors would also like to thank Mr. T. Meadley (AMOK Ltd., Saskatoon) for his cooperation throughout this study. Finally, the authors would like to acknowledge the assistance of some of the staff at Cluff Lake Mining during this field investigation.

REFERENCES

1. Blanc, C., Fontan, J., Chapuis, A., Billard, F., Madelaine, G. and Pradel, J., "Dosage du radon et de ses descendants dans une mine d'uranium - repartition granulometrique des aerosols radioactifs"; in Assessment of Airborne Radioactivity, IAIA (Vienna), pp 229-237, 1967.

2. Busigin, A., Van der Vooren, A. and Phillips, C.R., "Attached and unattached radon daughters: measurements and measurement techniques in uranium mines and in the laboratory"; AECB Report; 1978.

3. Jacobi, W. Biophysik, vol 1, p. 175; 1963.

4. Mercer, T.T. and Stowe, W.A., "Radioactive aerosols produced by radon in room air"; in Inhaled Particles III, vol 2, Unwin Brothers Ltd., W.H. Walton (Ed.); 1971.

5. Bigu, J. and Grenier, M.G., "Studies of radioactive dust in Canadian uranium mines"; CIM Bull., vol. 77, pp. 62-68; 1984.

6. Duport, P.J. and Edwardson, E., "Characterization of radioactive long-lived dust present in uranium mine and mill atmospheres"; in Proc Occup Radiation Safety in Mining, vol. 1. pp 189-195; Canadian Nuclear Association (Toronto), H. Stocker (Ed.); 1985.

7. Bigu, J. and Grenier, M.G., "Characterization of radioactive dust in Canadian underground uranium mines"; Proc 2nd Ventilation Congr, Reno, Nevada, pp 269-277; A.A. Balkema, Rotterdam, P. Mousset-Jones (Ed.); 1985.

8. Bigu, J. and Edwardson, E., "Characterisation of long-lived radioactive dust emissions in physico-chemical operations in an uranium mill"; Division Report M&ET/MRL 86- (TR); CANMET, Energy, Mines and Resources Canada; 1986.

Table 1 - Cascade impactors operating characteristics

Impactor	Sampling Flow-rate L/min	Stage Number	Cut-Off Size μm
EMR*	3.3	1	26
		2	16
		3	6.4
		4	3.8
		5	2.5
		6	1.4
		7	0.8
		8	0.5
		9	0.3
		10	0.06
C	10.5	1	14.8
		2	8.8
		3	3.5
		4	2.1
		5	1.4
		6	0.8
		7	0.4
		8	0.23
M_2	2.0	1	21.3
		2	14.8
		3	9.8
		4	6.0
		5	3.5
		6	1.55
		7	0.93
		8	0.52

* In June, the EMR impactor was operated at a sampling flow-rate of 10.5 L/min. The cut-off sizes for this case are the same as those corresponding to C.

Table 2 - Cascade impactors data for several mechanical operations in a uranium mill.

Mechanical Operation	Date 1985	Impactor	MMAD µm	Dust σg	AMAD(LLRD) µm	LLRD σg	AMAD(RnD) µm	RnD σg	Dust Conc. mg/m^3	LLRD Conc. mBq/m^3	LLRD(S.A.) mBq/mg
Grizzly (TP1)	March 22	C	15.4	2.8	15.3	3.4	0.66	9.1	12.51	1090	87
" "	"	EMR	14.5	2.4	19.0	3.0	0.69	2.6	8.99	1570	175
Jaw Crusher (TP2)	March 23	C	12.8	3.0	12.3	3.3	0.26	6.5	2.70	380	141
" " "	"	EMR	8.4	2.7	7.6	3.7	0.16	13.6	1.53	380	248
Cone Crusher (TP4)	March 25	C	5.4	2.6	5.7	2.8	-	-	0.84	190	226
" " "	"	EMR	6.6	2.4	6.2	3.4	-	-	0.86	270	314
Screens (TP3)	March 24	C	5.3	2.3	5.8	2.6	0.58	4.7	1.69	390	231
" "	"	EMR	6.2	2.4	5.7	3.0	0.69	4.6	1.49	520	349
Top Fine Ore Bin/	March 26	C	4.0	3.3	4.0	3.3	0.31	7.1	0.30	180	600
Conveyor Belt #8 (TP5)	"	EMR	3.7	4.5	4.1	3.5	0.14	13.6	0.37	230	605
	June 8	EMR	3.4	2.8	3.8	3.1	-	-	0.08	100	1250
Grinding (TP6)	June 5	EMR	-	-	3.7	5.8	0.20	10.5	-	48	-
	June 7	M_2	-	-	10.0	2.3	-	-	-	59	-
Yellowcake Packaging	March 22	C	10.5	3.1	11.1	3.5	-	-	12.43	1.3×10^5	1.05×10^4
(TP7)	"	EMR	12.3	3.7	11.8	2.6	-	-	6.21	1.25×10^5	2.01×10^4

Notes: a) C and EMR are Sierra impactors. M_2 is a Marple impactor.
b) σg represents geometric standard deviation (µm).
c) RnD stands for radon progeny.
d) S.A. indicates specific activity.

Table 3 - Alpha-particle energy corresponding to some members of the uranium and thorium natural radioactive chains.

Radioisotope	Symbol	α-Energy MeV	Remarks
Thorium	^{232}Th	4.08	Long-lived
Thorium	^{228}Th	5.52	" "
Radium	^{224}Th	5.79	" "
Thoron	^{220}Rn	6.28	Short-lived
Thorium A	^{216}Po	6.80	" "
Thorium C	^{212}Bi	6.05	" "
Thorium C'	^{212}Po	8.78	" "
Uranium	^{238}U	4.2	Long-Lived
Uranium	^{234}U	4.7	" "
Thorium	^{230}Th	4.7	" "
Radium	^{226}Ra	4.8	" "
Radon	^{222}Rn	5.49	Short-lived
Radium A	^{218}Po	6.0	" "
Radium C'	^{214}Po	7.68	" "
Radium F	^{210}Po	5.30	" "

Table 4 - Gamma-energy of some of the radioisotopes identified in dust samples from several mill mechanical operations.

Radioisotope	Symbol	γ-Energy keV	Remarks
Lead	^{210}Pb	46.50	Long-Lived (medium)
Thorium	^{234}Th	63.29	Long-Lived
		92.38	" "
		92.80	" "
Radium	^{226}Ra	185.99	Long-Lived
Lead	^{214}Pb	241.91	Short-Lived
		295.40	" "
		351.90	" "
Bismuth	^{214}Bi	609.32	Short-Lived

Table 5 - Total and respirable dust concentration during some milling mechanical operations.

Location	Total Dust[1] (mg/m^3)	Respirable Dust[2] (mg/m^3)
Jaw crusher (TP2)	2.16	0.28
Screens (TP3)	1.58	0.41
Cone crusher (TP4)	0.83	0.11
Conveyor Belt/ Fine Ore Bin (TP5)	0.23	0.16

[1] Using an open-face filter holder.

[2] Using a nylon cyclone.

Table 6 - Working Level measured by a WLM-300 continuous Working Level Monitor at several locations.

Location	Date	WL* (mWL)
Grizzly (TP1)	March 22-23/85	15.3±3.3
Jaw Crusher (TP2)	March 23-24/85	16.0±1.5
Cone Crusher (TP4)	March 25-26/85	48.4±4.2
Screens (TP3)	March 24-25/85	54.7±11.1
Conveyor Belt/ Fine Ore Bin (TP5)	March 26-27/85	66.5±5.0

* Average value calculated over a 14 h period.

Table 7 - Radon progeny grab-sampling data by Thomas-Tsivoglou method at several locations.

Location	Time	WL (mWL)	$[^{218}Po]$ (pCi/L)	$[^{214}Pb]$ (pCi/L)	$[^{214}Bi]$ (pCi/L)	$[^{214}Pb]/[^{218}Po]$	$[^{214}Bi]/[^{218}Po]$	Date
Grizzly (TP1)	18:05	4.0	1.49	0.34	0.21	0.23	0.14	March 22/85
	20:44	5.8	2.96	0.19	0.48	0.06	0.16	"
	21:57	9.3	5.52	0.62	0.12	0.11	0.02	"
Jaw Crusher (TP2)	20:23	13.4	3.78	1.58	0.41	0.42	0.11	March 23/85
	20:58	13.3	1.69	1.20	1.46	0.71	0.86	"
	21:35	16.8	5.56	1.42	1.03	0.26	0.19	"
	22:10	18.4	6.73	1.79	0.64	0.27	0.10	"
Screens (TP3)	20:36	33.7	11.57	3.45	1.15	0.30	0.10	March 24/85
	21:12	36.5	14.66	4.25	-0.05	0.29	-	"
	21:47	34.7	9.92	2.73	2.85	0.28	0.29	"
	22:25	34.1	12.01	3.36	1.25	0.28	0.10	"
Yellowcake Packaging* (TP7)	19:57	19.6	0.95	2.68	1.34	2.82	1.41	March 22/85
	20:55	15.1	-1.79	1.02	3.16	-	-	"
	21:36	14.1	-0.18	0.41	3.28	-	-	"

* Data calculated assuming α-count recorded as originating from ^{218}Po and ^{214}Po.

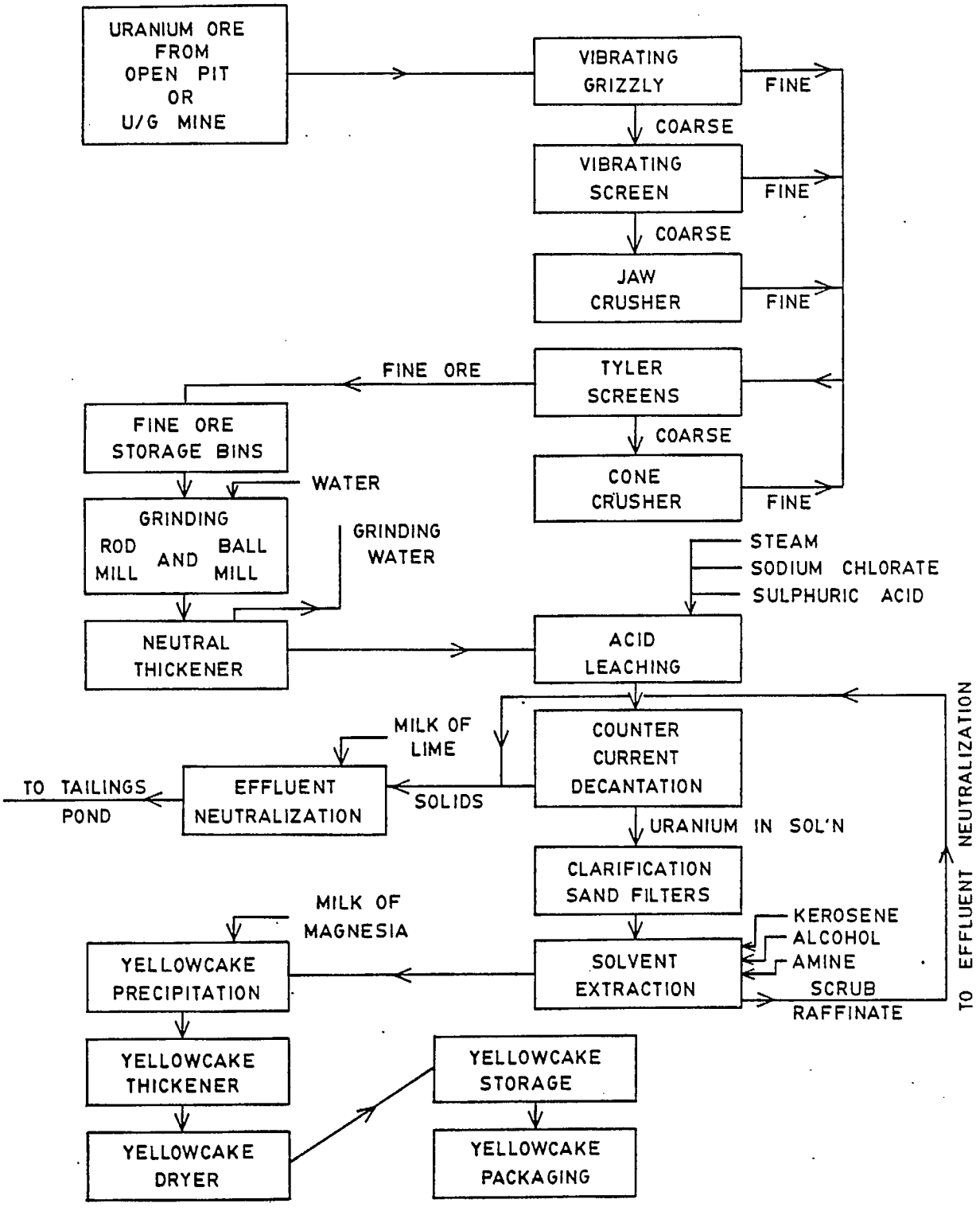

Fig. 1 - Block diagram of mechanical and physico-chemical operations in a uranium mill.

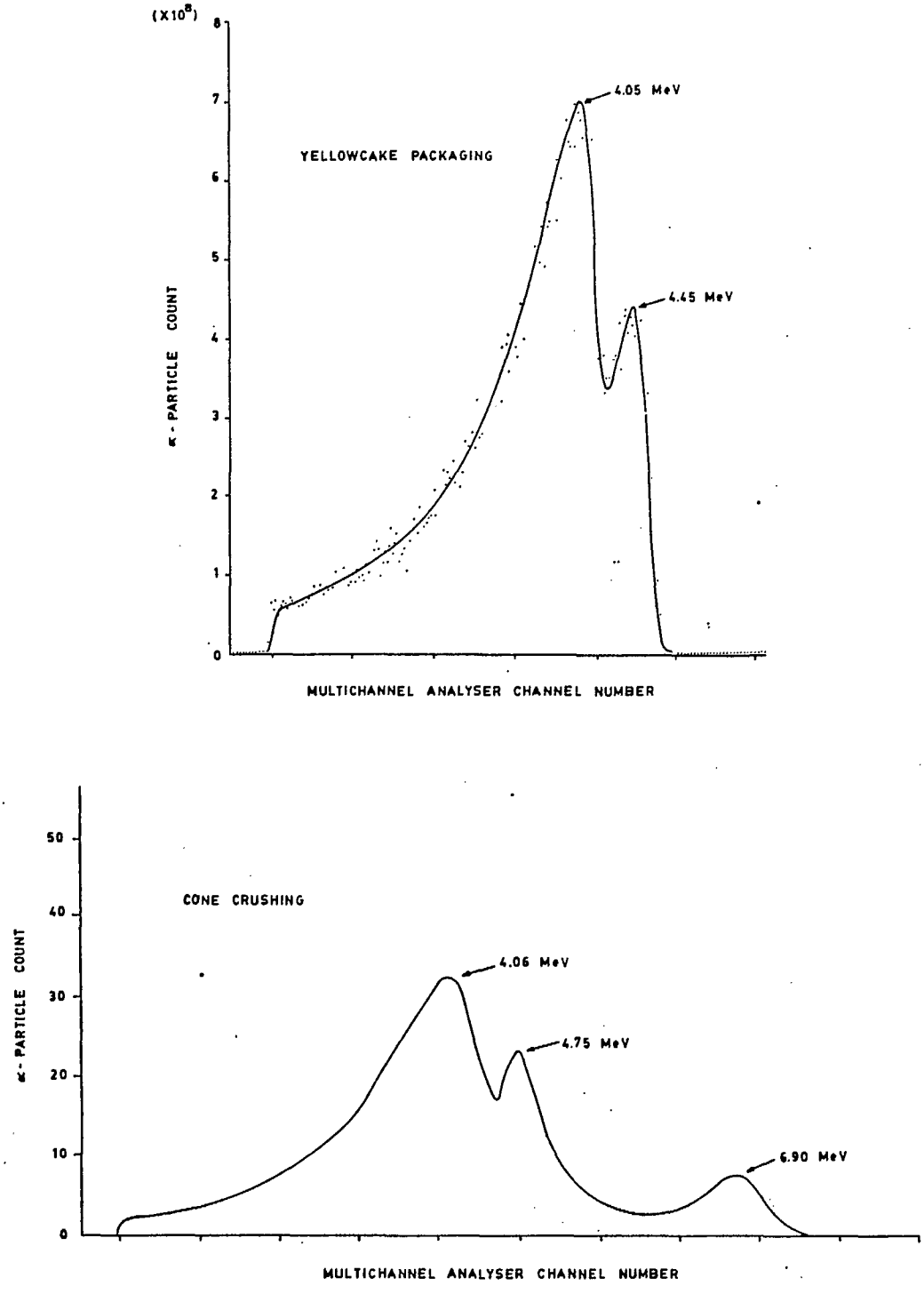

Fig. 2 - Alpha-particle spectra corresponding to different mill operations.

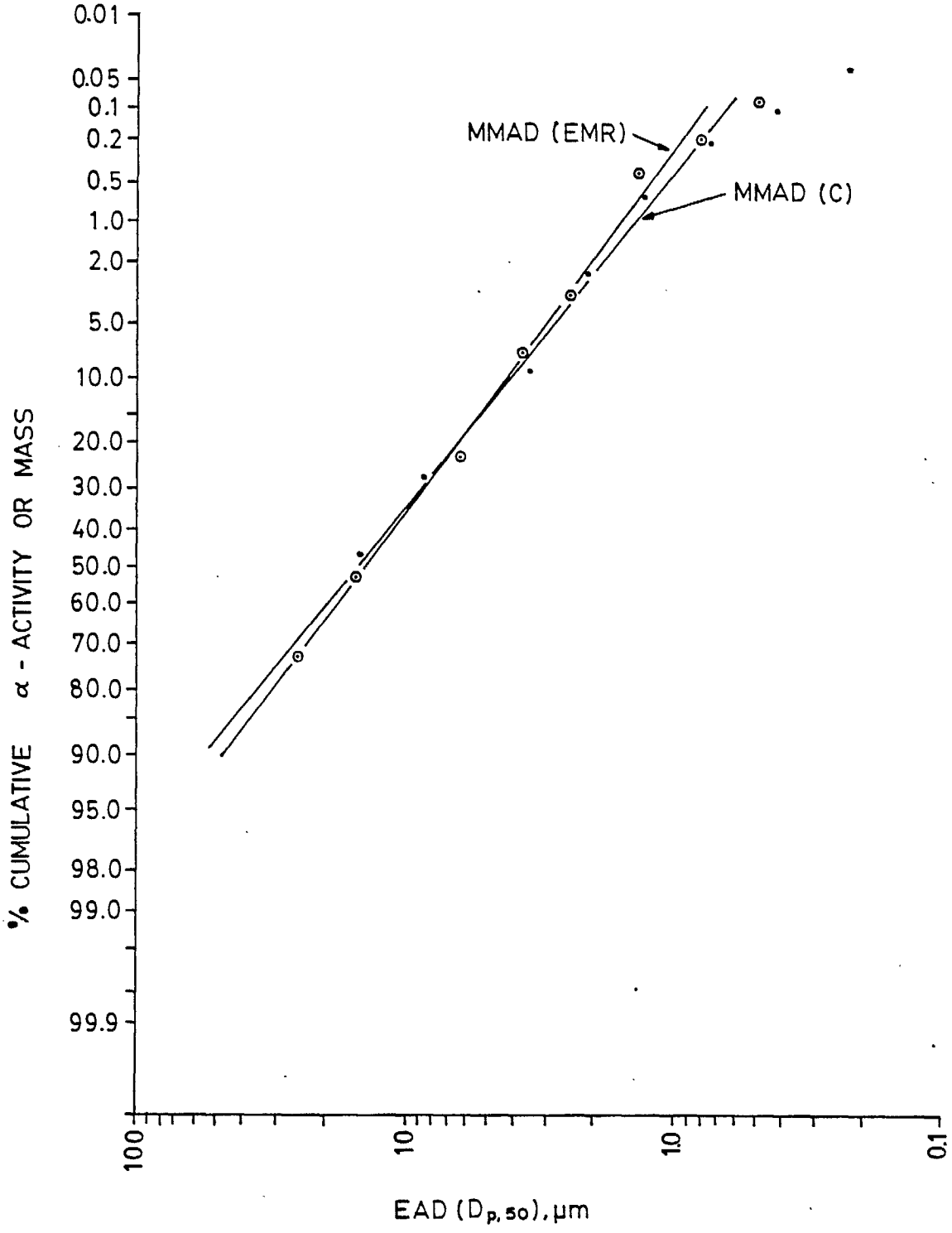

Fig. 3 - Percentage cumulative dust versus EAD for the 'grizzly' fragmentation operation.

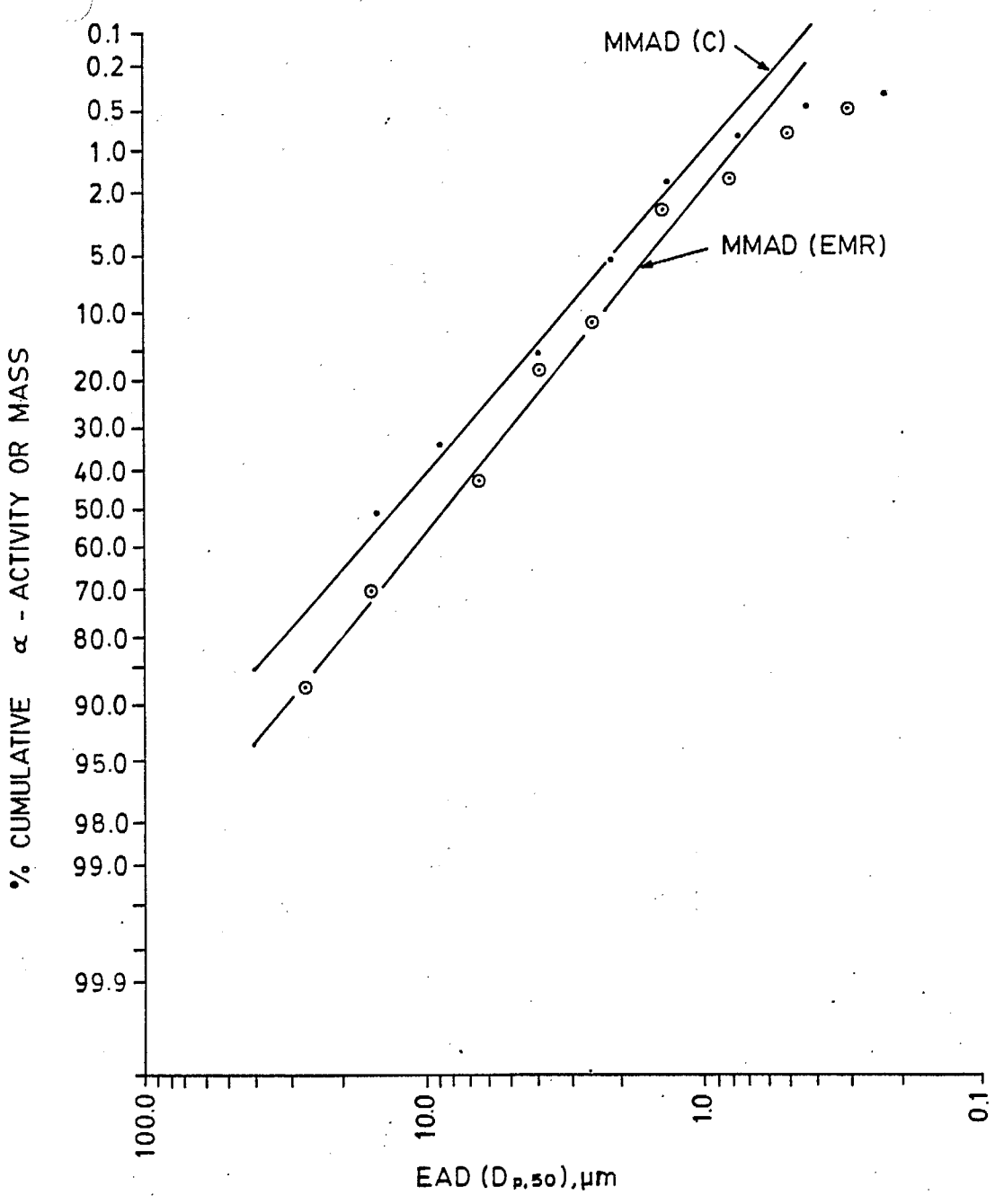

Fig. 4 - Percentage cumulative dust versus EAD for the jaw crusher operation.

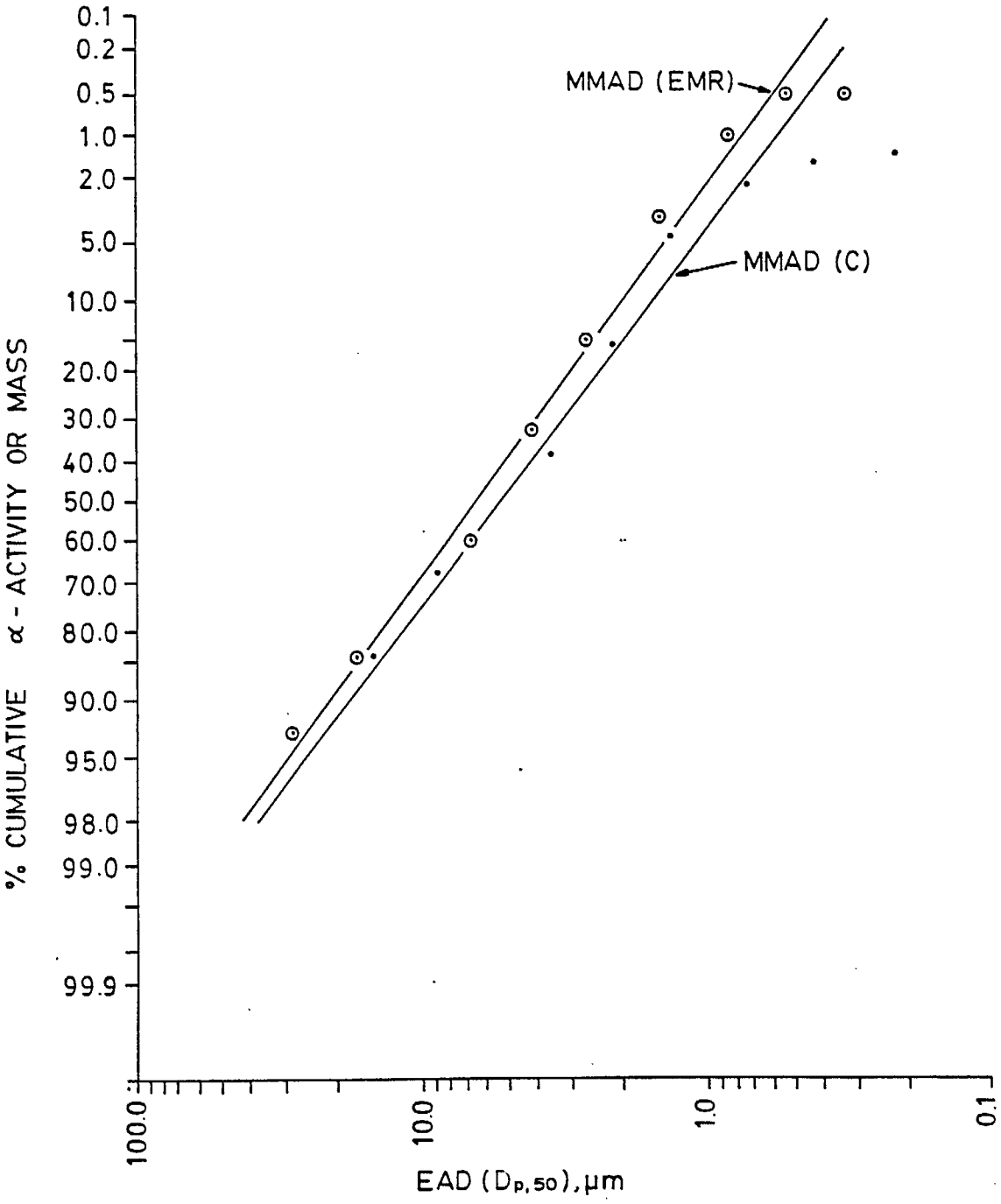

Fig. 5 - Percentage cumulative dust versus EAD for the cone crusher operation.

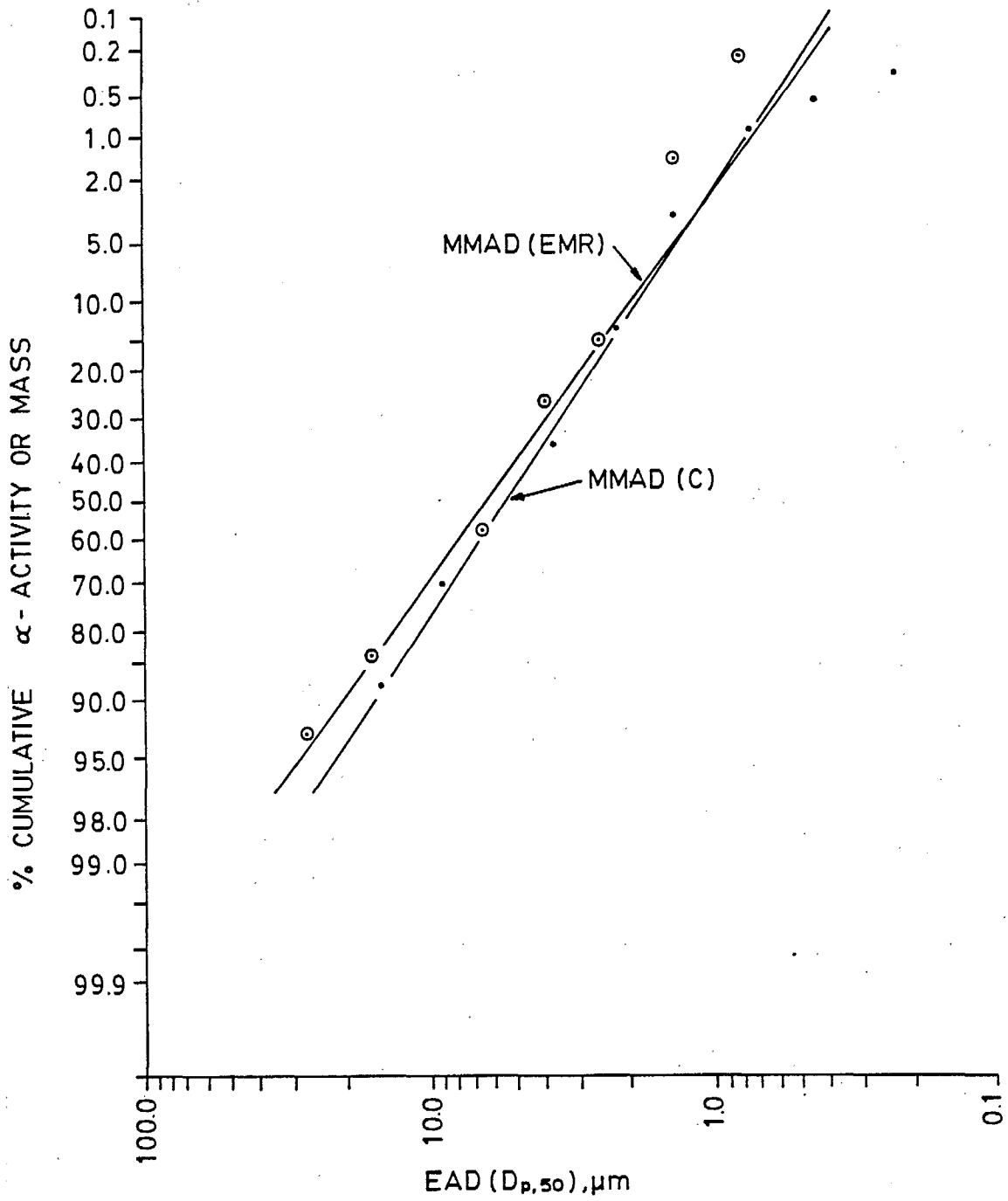

Fig. 6 - Percentage cumulative dust versus EAD for screening operations.

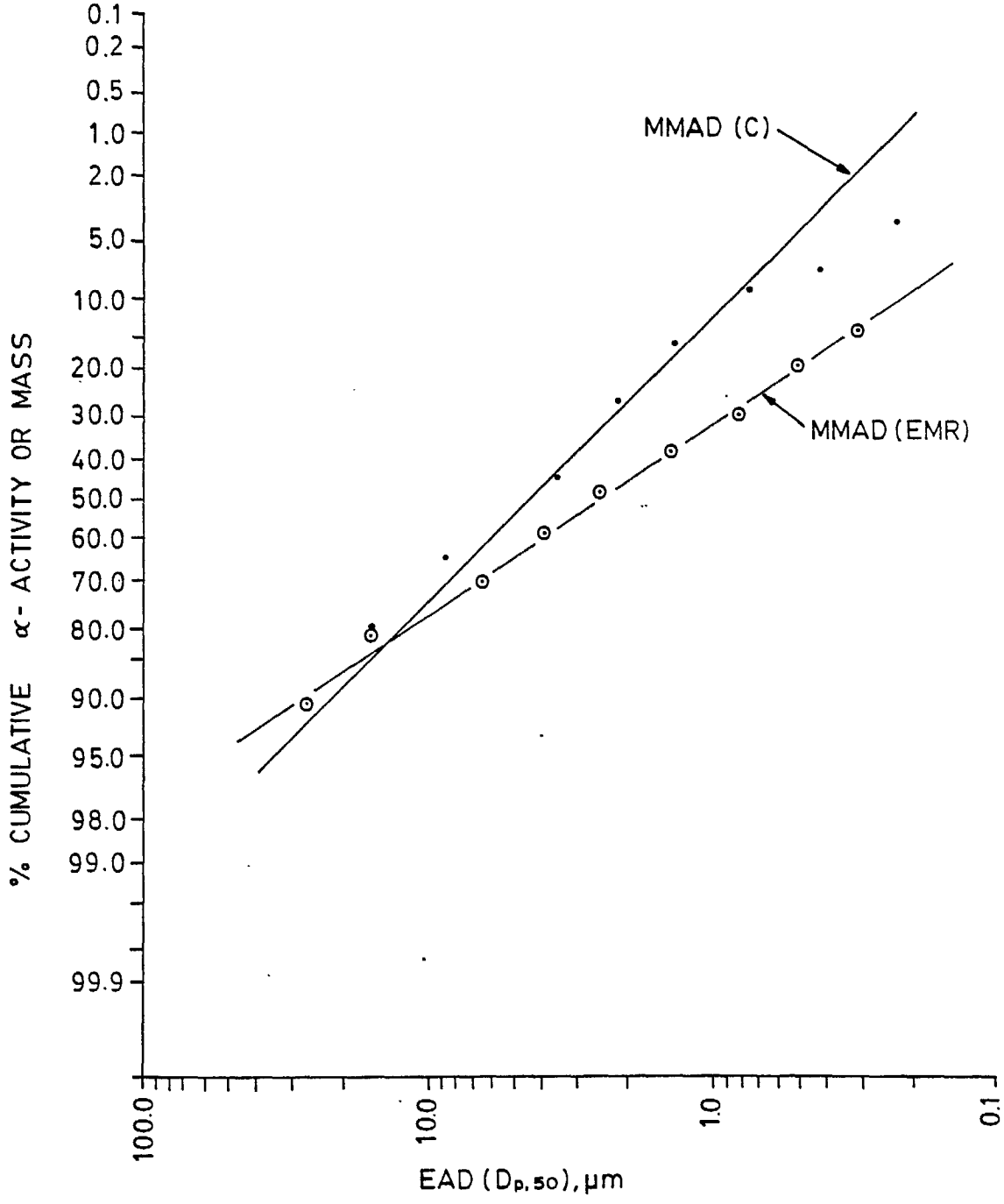

Fig. 7 - Percentage cumulative dust versus EAD for the fine ore bin/conveyor belt.

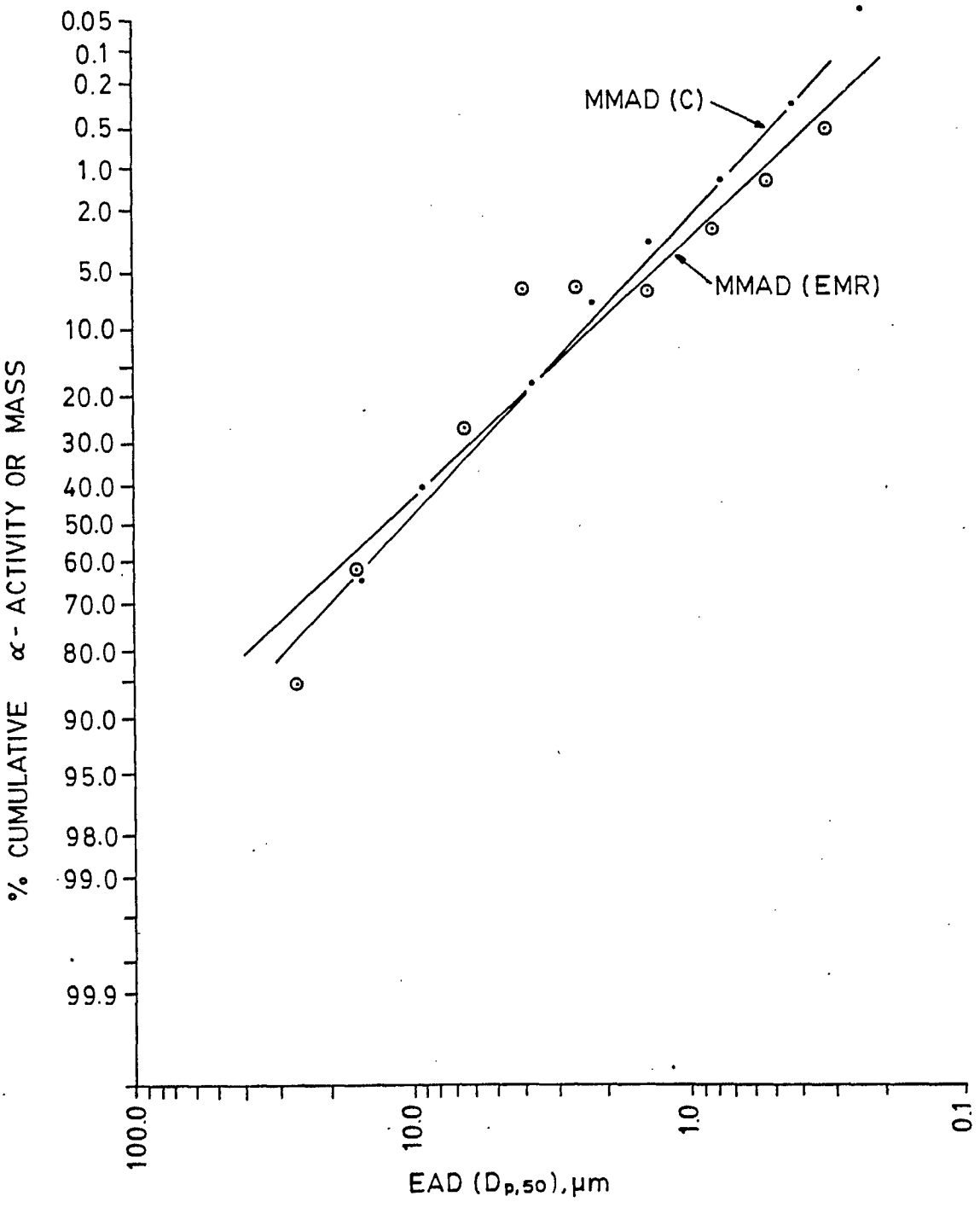

Fig. 8 - Percentage cumulative dust versus EAD for the yellowcake packaging operation.

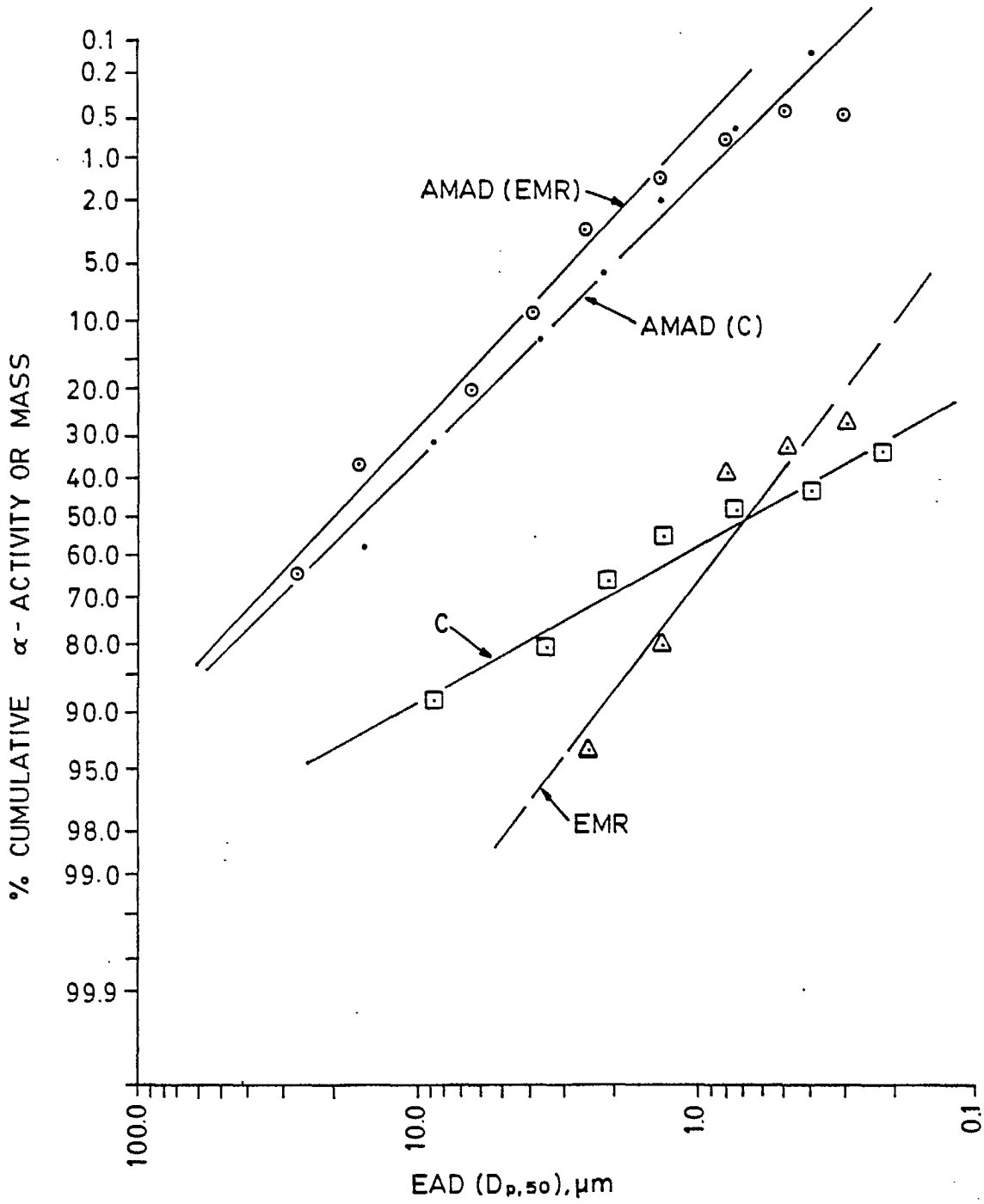

Fig. 9 - Percentage cumulative LLRD (upper graphs) and radon progeny (lower graphs) α-activity versus EAD for the 'grizzly' fragmentation operation.

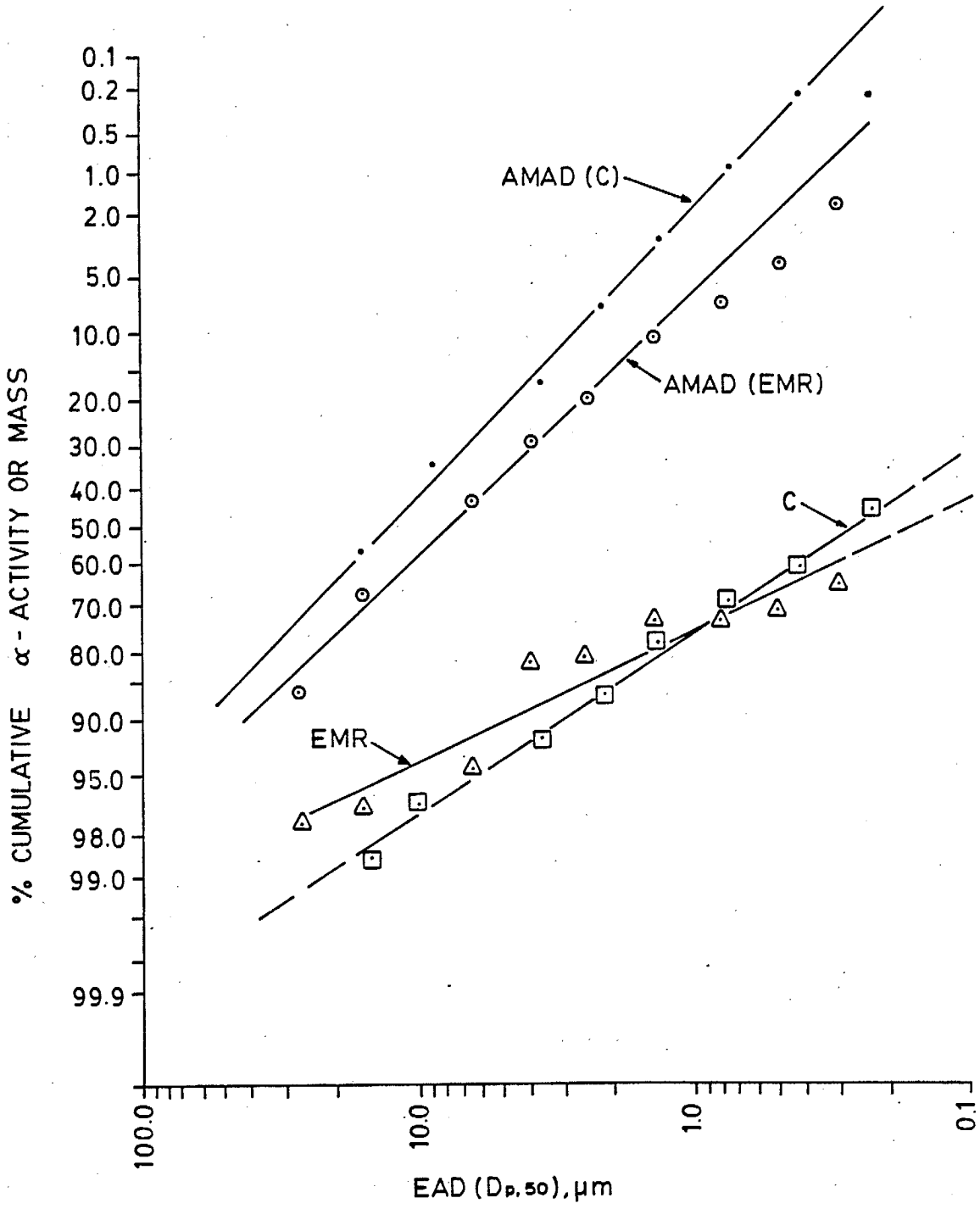

Fig. 10 - Percentage cumulative LLRD (upper graphs) and radon progeny (lower graphs) α-activity versus EAD for the jaw crusher.

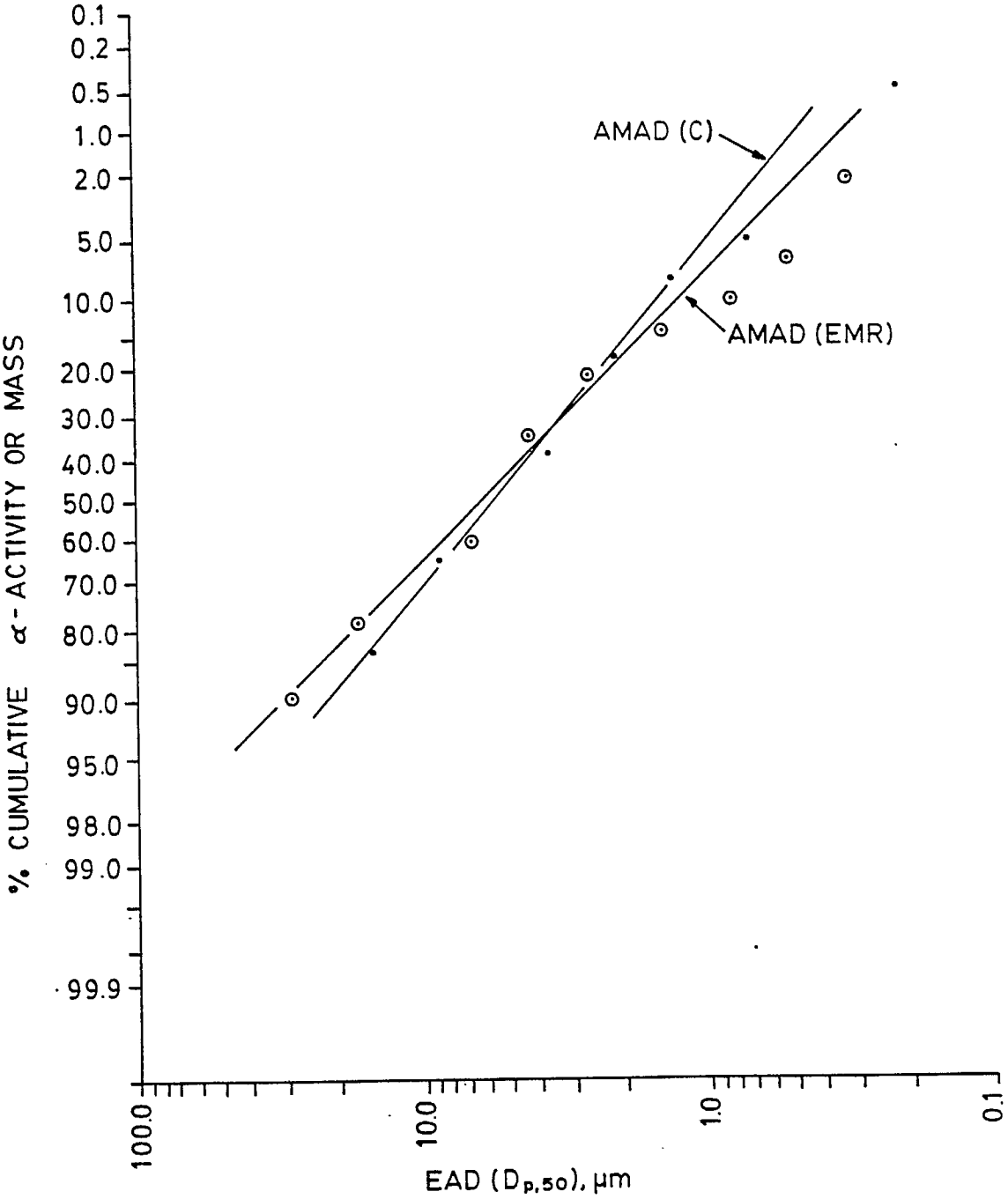

Fig. 11 - Percentage cumulative LLRD α-activity versus EAD for the cone crusher.

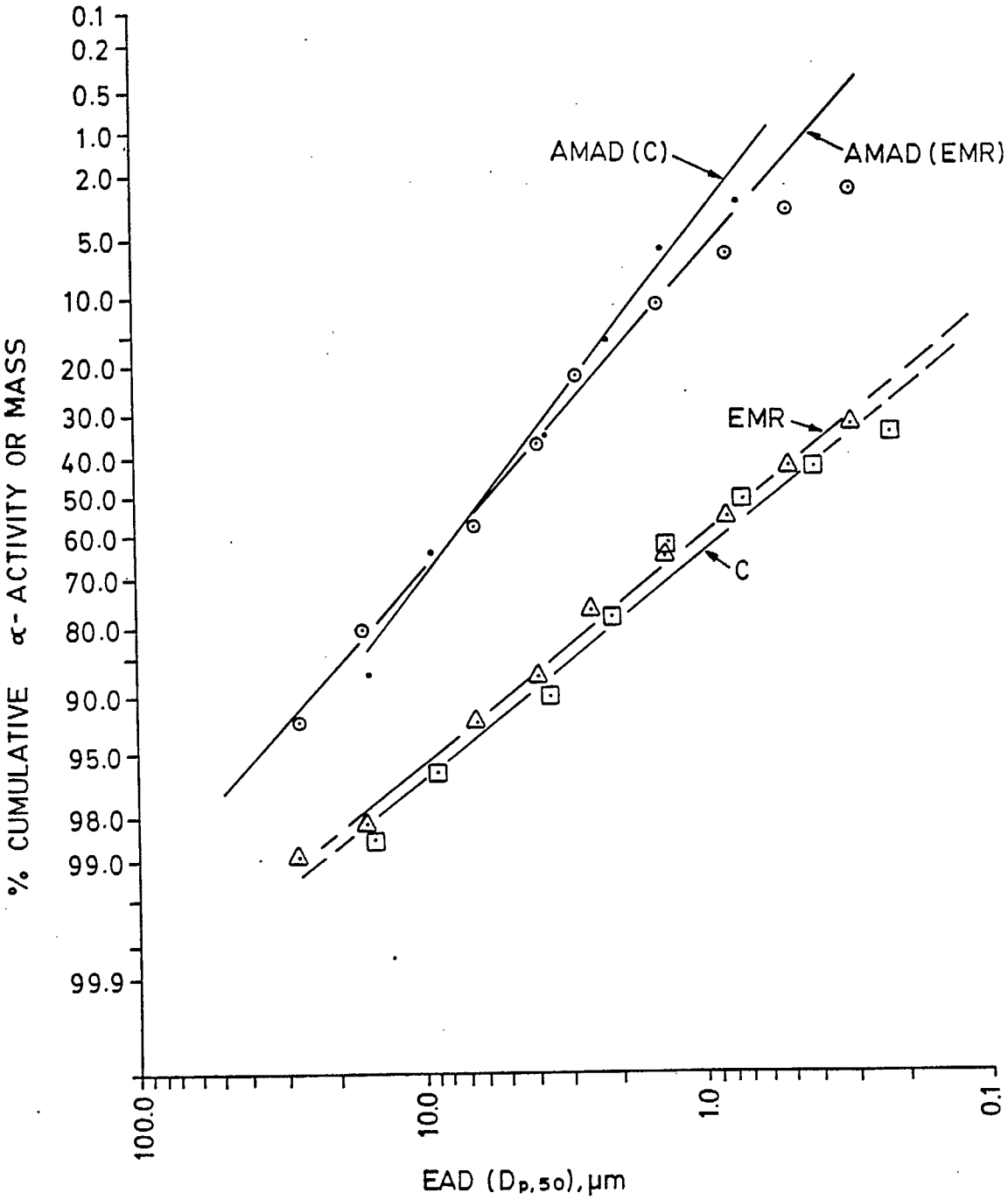

Fig. 12 - Percentage cumulative LLRD (upper graphs) and radon progeny (lower graphs) α-activity versus EAD for the screening operations.

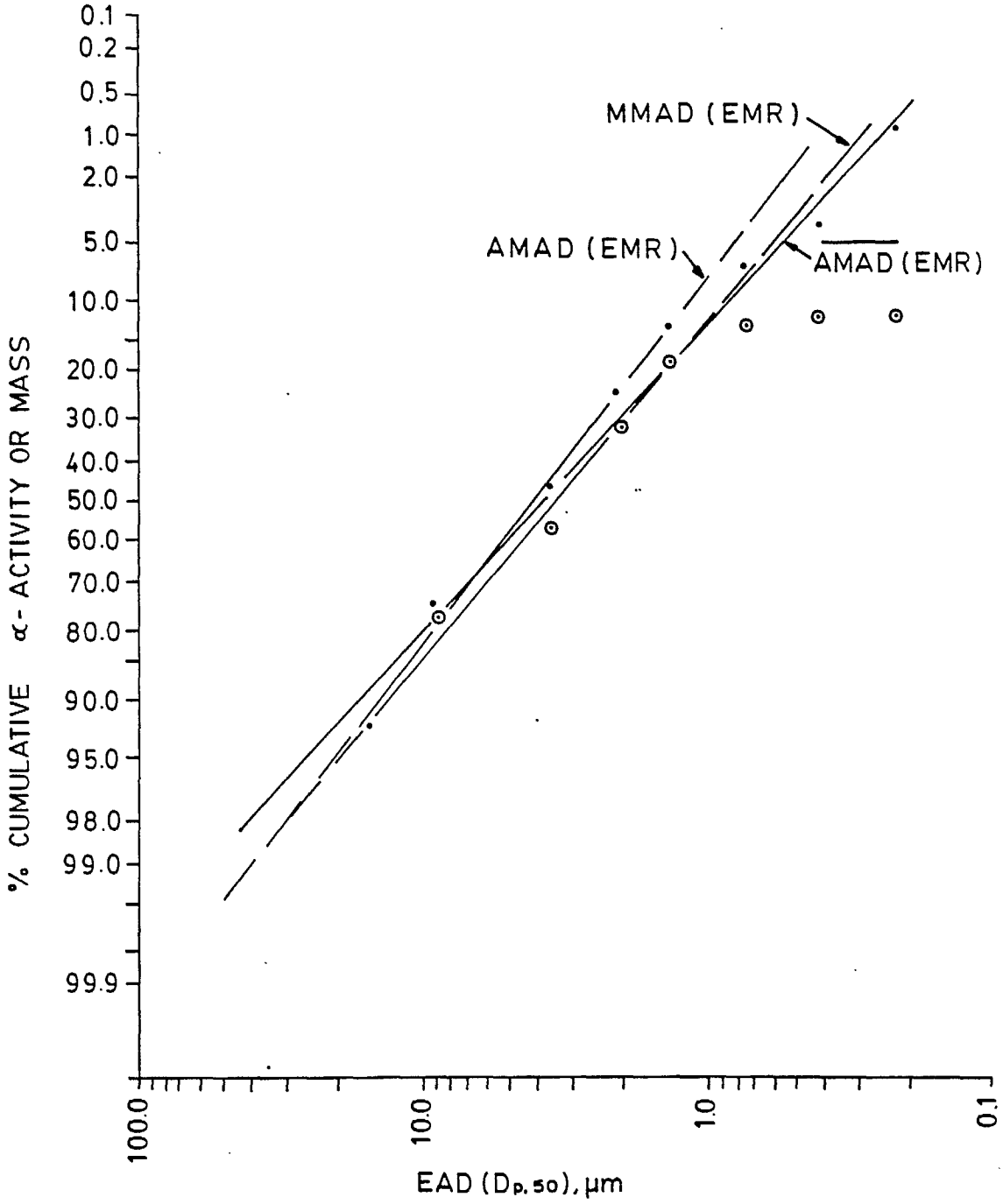

Fig. 13 - Percentage cumulative dust (MMAD) and percentage cumulative LLRD (AMAD) α-activity versus EDA for the fine ore bin/conveyor belt operation.

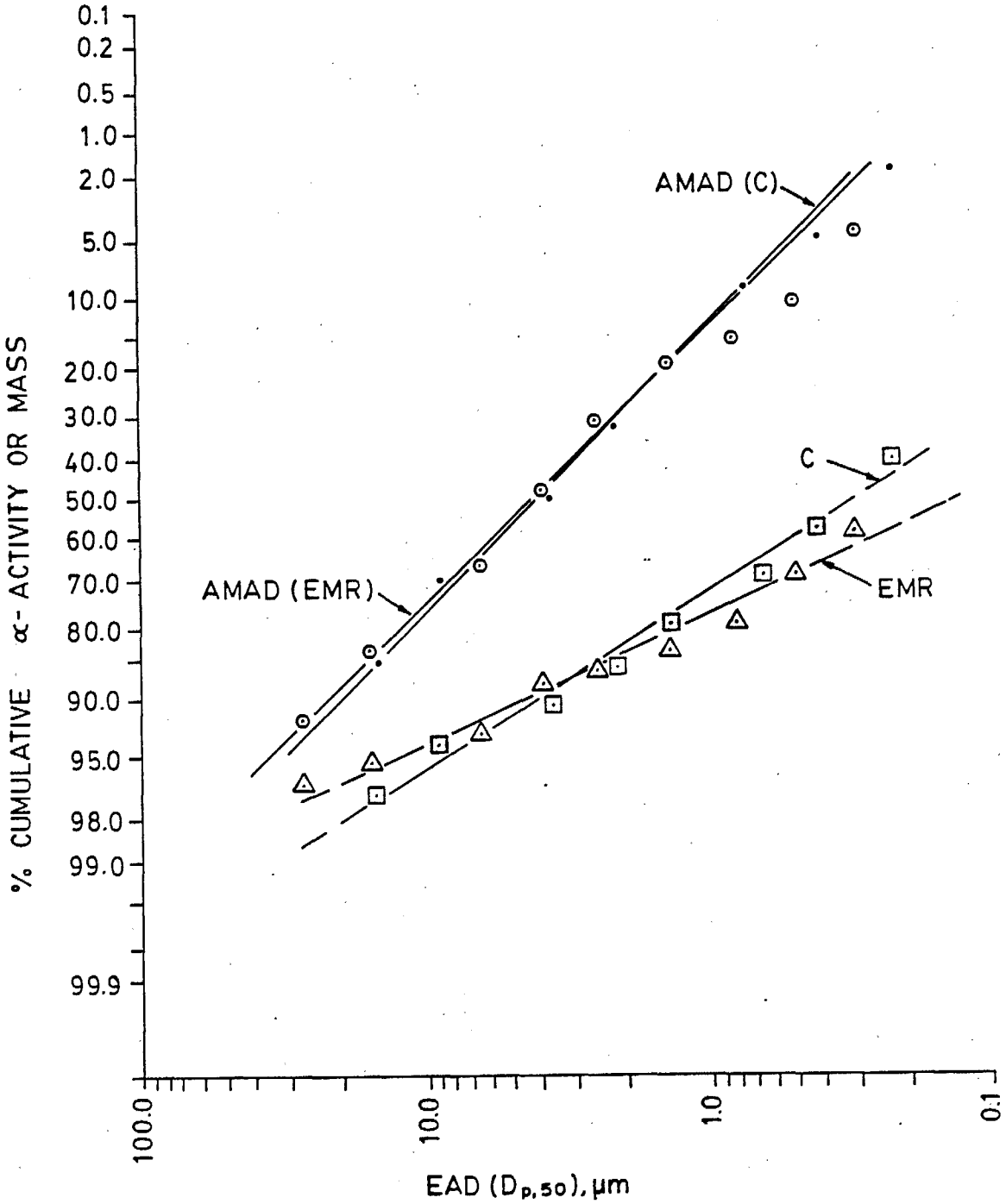

Fig. 14 - Percentage cumulative LLRD (upper graphs) and radon progeny (lower graphs) α-activity versus EAD for the fine ore bin/conveyor belt operation.

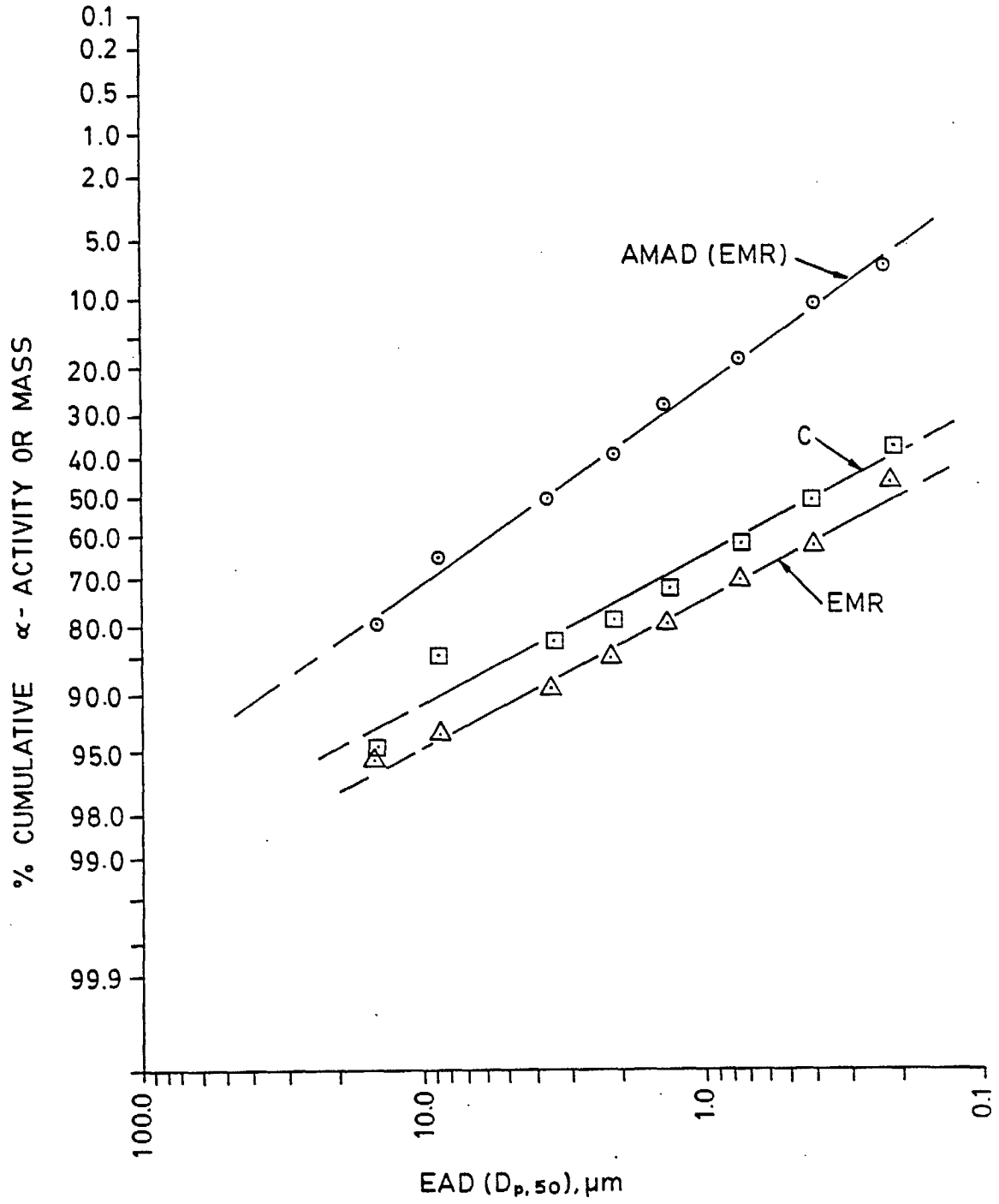

Fig. 15 - Percentage cumulative LLRD (upper graph) and radon progeny (lower graphs) α-activity versus EAD for the grinding operation.

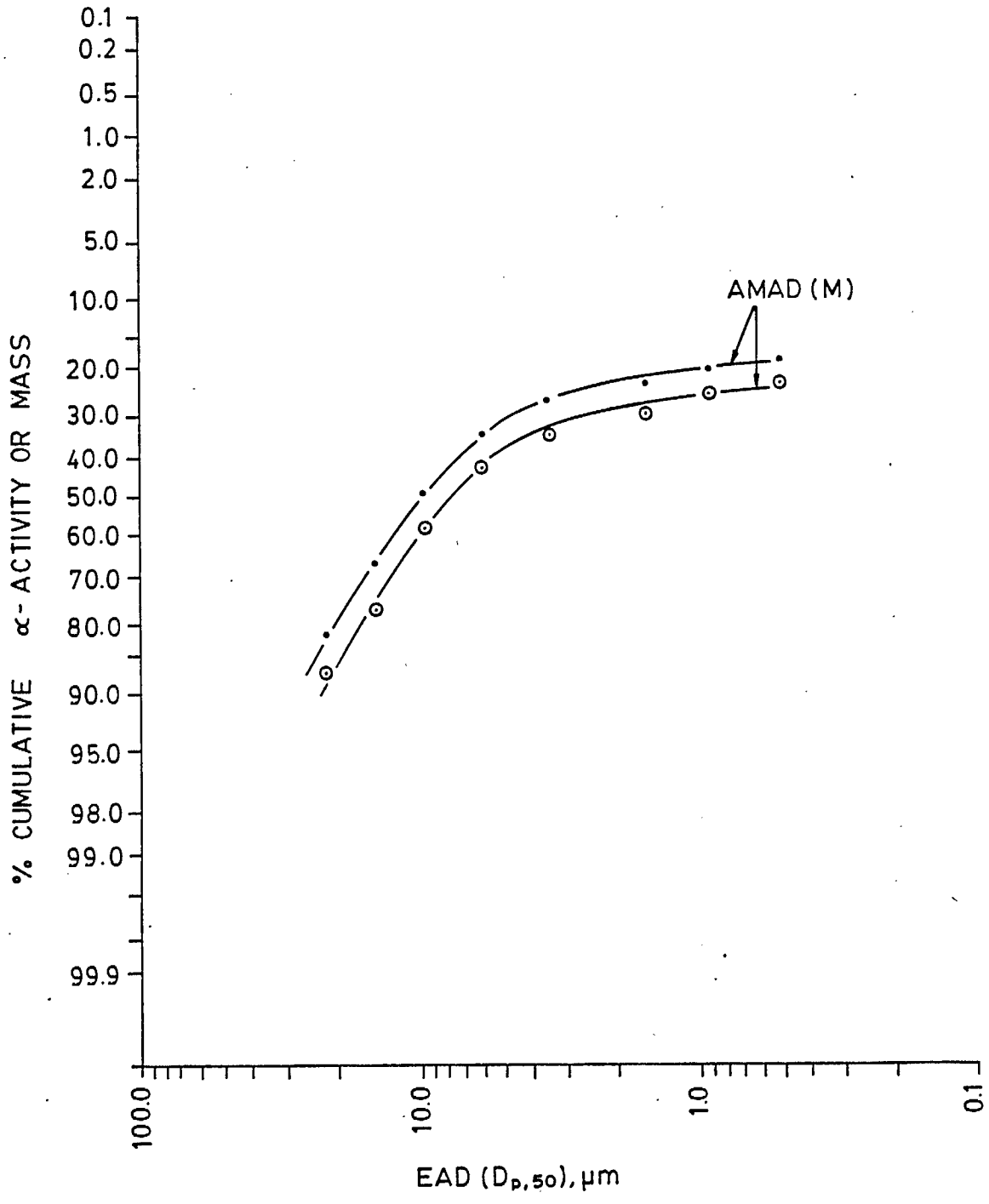

Fig. 16 - Percentage cumulative LLRD α-activity versus EAD for the grinding operation. (Note: the upper graph has been corrected for impactor stage collection efficiency. The lower graph shows non-corrected values.)

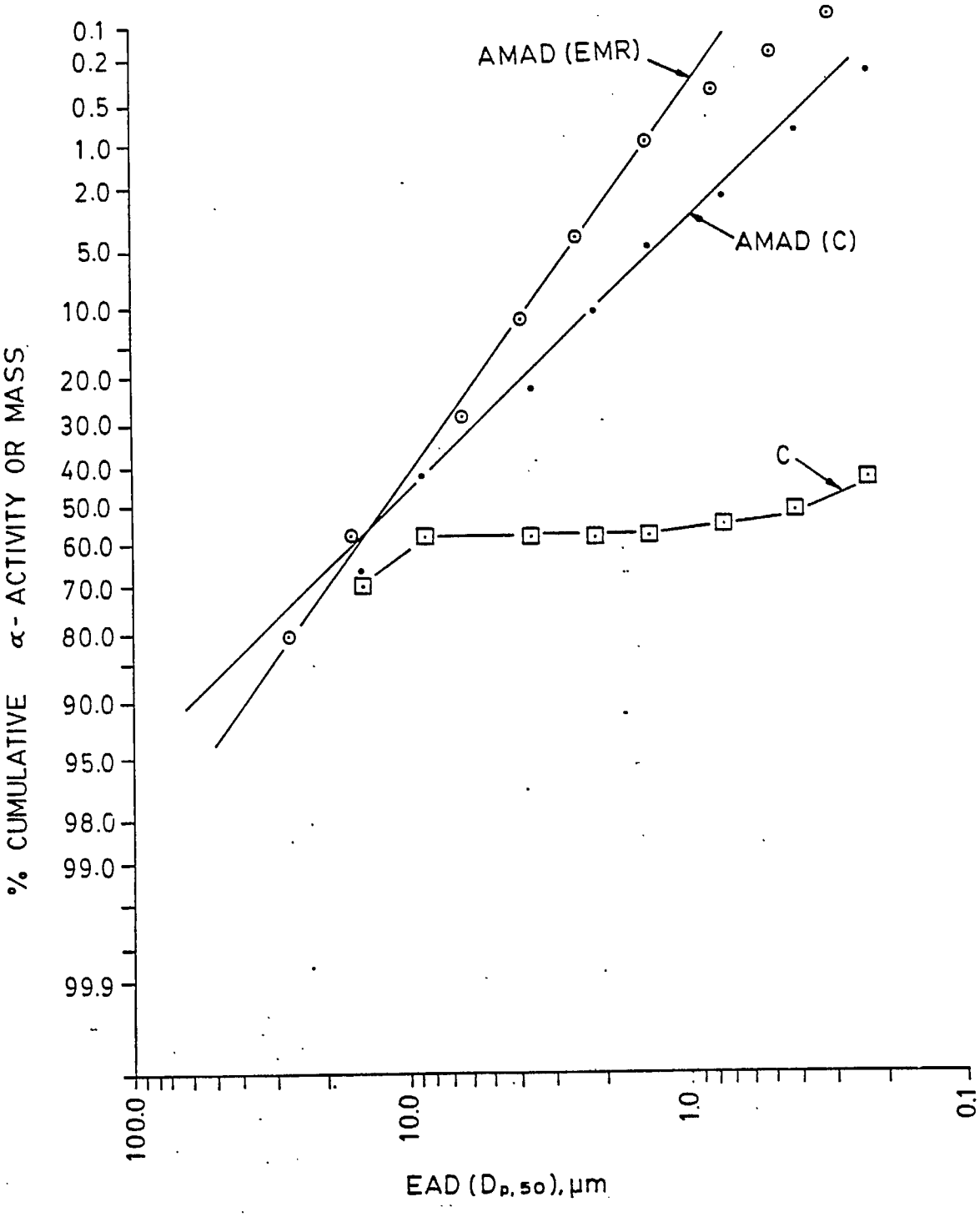

Fig. 17 - Percentage cumulative LLRD α-activity versus EAD for the yellowcake packaging operation.